ornl

OAK RIDGE NATIONAL LABORATORY

MARTIN MARIETTA

ORNL/TM-11532

MARTIN MARIETTA ENERGY SYSTEMS LIBRARIES

3 4456 0348646 7

Investigation of Radiation Effects in Hiroshima and Nagasaki Using a General Monte Carlo-Discrete Ordinates Coupling Scheme

S. N. Cramer
C. O. Slater

OAK RIDGE NATIONAL LABORATORY
CENTRAL RESEARCH LIBRARY
CIRCULATION SECTION
4500N ROOM 175
LIBRARY LOAN COPY
DO NOT TRANSFER TO ANOTHER PERSON
If you wish someone else to see this report, send in name with report and the library will arrange a loan.

OPERATED BY
MARTIN MARIETTA ENERGY SYSTEMS, INC
FOR THE UNITED STATES
DEPARTMENT OF ENERGY

This report has been reproduced directly from the best available copy.

Available to DOE and DOE contractors from the Office of Scientific and Technical Information, P.O. Box 62, Oak Ridge, TN 37831; prices available from (615) 576-8401, FTS 626-8401.

Available to the public from the National Technical Information Service, U.S. Department of Commerce, 5285 Port Royal Rd., Springfield, VA 22161.
NTIS price codes—Printed Copy: A03 Microfiche A01

This report was prepared as an account of work sponsored by an agency of the United States Government. Neither the United States Government nor any agency thereof, nor any of their employees, makes any warranty, express or implied, or assumes any legal liability or responsibility for the accuracy, completeness, or usefulness of any information, apparatus, product, or process disclosed, or represents that its use would not infringe privately owned rights. Reference herein to any specific commercial product, process, or service by trade name, trademark, manufacturer, or otherwise, does not necessarily constitute or imply its endorsement, recommendation, or favoring by the United States Government or any agency thereof. The views and opinions of authors expressed herein do not necessarily state or reflect those of the United States Government or any agency thereof.

ORNL/TM-11532

Radiation Shielding Information Center

Engineering Physics and Mathematics Division

Investigation of Radiation Effects in Hiroshima and Nagasaki Using a General Monte Carlo-Discrete Ordinates Coupling Scheme

S. N. Cramer

C. O. Slater

DATE PUBLISHED – May 1990

Prepared for the
DEFENSE NUCLEAR AGENCY
under Interagency Agreement Number 0046-C084-A1

Prepared by the
OAK RIDGE NATIONAL LABORATORY
Oak Ridge, Tennessee 37831
operated by
MARTIN MARIETTA ENERGY SYSTEMS, INC.
for the
U.S. DEPARTMENT OF ENERGY
under contract DE-AC05-89OR21400

MARTIN MARIETTA ENERGY SYSTEMS LIBRARIES

3 4456 0348646 7

CONTENTS

1. INTRODUCTION 1
2. RADIATION TRANSPORT COUPLING METHODS 2
3. NAGASAKI BUILDING CALCULATION 11
4. HIROSHIMA NUCLIDE ACTIVATION CALCULATIONS 15
5. CODING DETAILS AND CONCLUDING REMARKS 16
APPENDIX A 19
REFERENCES 23

LIST OF FIGURES

Figure		Page
1	Coupling system geometry	3
2	Monte Carlo geometry and discrete ordinates flux grid	5
3	Horizontal projection of the coupling system geometry	7
4	Discrete ordinates angular system	8
5	Reinforced concrete building in Nagasaki (Chinzei School, used as a factory machine shop)	12
6	Computer mock-up of a reinforced concrete building in Nagasaki	13

Abstract

A general Monte Carlo-discrete ordinates radiation transport coupling procedure has been created to study effects of the radiation environment in Hiroshima and Nagasaki due to the bombing of these two cities. The forward two-dimensional free-field air-over-ground flux is coupled with an adjoint Monte Carlo calculation. The size, orientation, or translation of the Monte Carlo geometry is unrestricted. The radiation effects calculated are the dose in the interior of a large concrete building in Nagasaki and the activation production of Co-60 and P-32 in Hiroshima.

1. INTRODUCTION

A general Monte Carlo-discrete ordinates radiation transport calculational scheme has been created to study effects of the radiation environment in Hiroshima and Nagasaki due to the bombing of these two cities. Various such studies for comparison with physical data have progressed since the end of World War II with advancements in computing machinery and computational methods. These efforts have intensified in the last several years with the U.S.-Japan joint reassessment of nuclear weapon dosimetry in Hiroshima and Nagasaki.[1] Three principal areas of investigation are: (1) to determine by experiment and calculation the neutron and gamma ray energy and angular spectra and total yield of the two weapons, (2) using these weapons descriptions as source terms, to compute radiation effects at several locations in the two cities for comparison with experimental data collected at various times after the bombings and thus validate the source terms, and (3) to compute radiation fields at the known locations of fatalities and surviving individuals at the time of the bombings and thus establish an absolute cause-and-effect relationship between the radiation received and the resulting injuries to these individuals and any of their descendants as indicated by their medical records.

It is in connection with the second and third items, the determination of the radiation effects and the dose received by individuals, with which the current study is concerned. In Hiroshima the activation products of several nuclides, such as Co-60 in iron components on building rooftops and P-32 in the sulfur in electric insulators on utility poles, have been measured and recorded as a function of radial position from ground zero in an effort to correlate the weapon source with the induced activation.

The study of radiation dose to individuals has always been more concentrated in Nagasaki, due primarily to the simpler and easily simulated "Fat Man" weapon in contrast to the more complicated "Little Boy" weapon in Hiroshima. The effort in Nagasaki has been further restricted to large, earthquake-proof concrete buildings a few hundred meters from ground zero. Here, in addition to the fatalities, many individuals survived in the lower floors of these buildings with radiation-only injuries. At other locations and in other structures where there was significant radiation, injuries to all individuals was complicated by structural collapse, flying debris, burns, etc., greatly complicating any correlations between radiation dose and resulting injuries.

2. RADIATION TRANSPORT COUPLING METHODS

A standard method for computing a radiation effect λ, such as one of those described above, is from

$$\lambda = \int_{\bar{n}\cdot\bar{\Omega}>0} \phi(\rho)\phi^*(\rho)(\bar{n}\cdot\bar{\Omega})d\rho \ , \tag{1}$$

where ρ represents the space, energy, and angular variables on some coupling surface completely surrounding the location in question. The radiation direction at the surface is $\bar{\Omega}$ and $\bar{n}$ is the normal direction at the surface into the volume containing the location. The forward particle flux $\phi(\rho)$ is computed by the two-dimensional discrete ordinates code DOT[2] to simulate the weapon as a point source in the cylindrical air-over-ground geometry, applicable to the entire Hiroshima area and most of Nagasaki (see Chapter 3 in Ref. 1, Vol. 1). The adjoint flux $\phi^*(\rho)$ times the cosine $\bar{n}\cdot\bar{\Omega}$ is computed by the multigroup Monte Carlo code MORSE[3] as the adjoint current at the coupling surface. Any complicated geometry inside the coupling surface can be modeled in three-dimensional detail. The geometry of the complete system is shown in Fig. 1. The two dimensional discrete ordinates system is defined by the $\bar{r}, \bar{z}$ coordinate axes, where the radial axis $\bar{r}$ coincides with the $\bar{x}$ axis and is perpendicular to the $\bar{y}$ axis. The three-dimensional Monte Carlo system is contained within the cylindrical volume element defined by $\Delta r, \Delta z$, and $\Delta\psi$. In the application here for the two Japanese cities, the $\bar{x}, \bar{y}$ plane represents the air-ground interface. The point S on the $\bar{z}$ axis is the weapon detonation location above ground zero, the $\bar{x}, \bar{y}, \bar{z}$ coordinate system origin.

Implicit in the application of Eq. (1) is the assumption that the coupling surface is placed several mean-free-paths away from the interior geometry to be modeled in detail. This placement of the coupling surface, known as the "surface integral approximation," is done to ensure that the interior geometry would not have perturbed the free field flux at the coupling surface if it could have been included in the free field calculation.

The coupling between the two systems is at point P' at the outer boundary of the Monte Carlo geometry shown within the volume element in Fig. 2. Here the point P_0 is the origin of the Monte Carlo geometry coordinate system $\bar{x}', \bar{y}', \bar{z}'$. This arbitrary system must first be rotated to align the $\bar{x}', \bar{y}', \bar{z}'$ axes parallel to and in the same sense of the $\bar{x}, \bar{y}, \bar{z}$ axes. It is then translated relative to P_c, the coupling reference point x_c, y_c, z_c in the $\bar{x}, \bar{y}, \bar{z}$ system. The point P_c' is the same as P_c, but x_c', y_c', z_c' are in the $\bar{x}', \bar{y}', \bar{z}'$ system. When the adjoint Monte Carlo particle escapes its geometry system at $P' = x', y', z'$ in direction $\bar{\Omega}'$, given by direction cosines U', V', W', then the coordinates, direction, and energy group must be converted to the discrete ordinates system in Fig. 1 so that the appropriate forward flux $\phi(\rho)$ can be determined in the evaluation of Eq. (1). This flux is determined by linear interpolation from the four fluxes at the corners of the $\Delta r_i \Delta z_j$ area containing P' in the $\bar{r}, \bar{z}$ plane. This grid of discrete ordinates fluxes must be large enough to

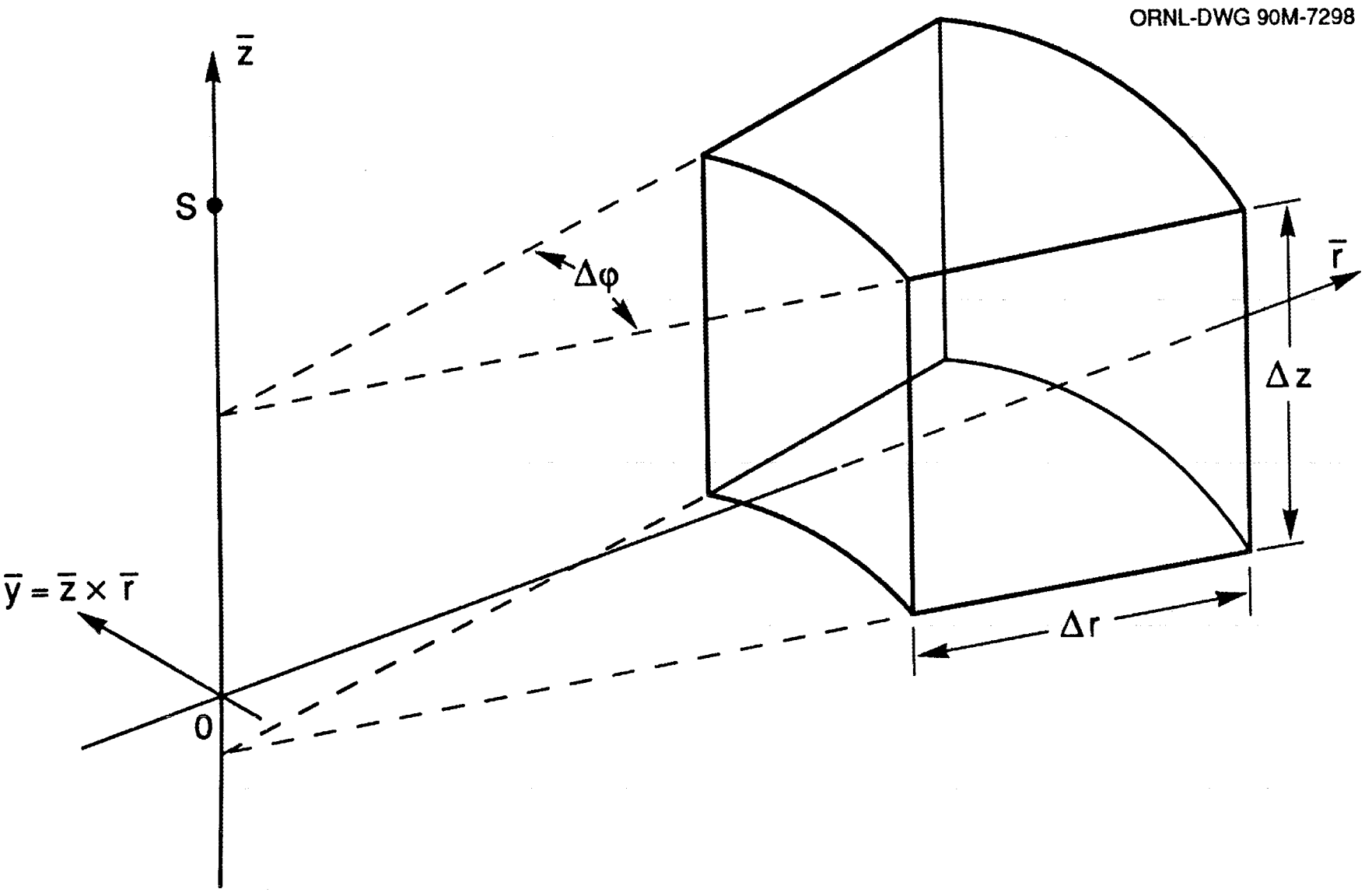

Figure 1. Coupling system geometry.

completely cover the Monte Carlo geometry when the grid is swept out through the angle $\Delta\psi$. The volume element created by this sweep is not done explicitly in the calculation, but only in an implicit manner in the coordinate and angle transformation. The locations of the node points in the grid correspond to the mid-points of the discrete ordinates calculational mesh. The points P_c and P_0 are not necessarily in the cylindrical element volume and may be chosen, along with the $\bar{x}', \bar{y}', \bar{z}'$ orientation, so that the Monte Carlo geometry may be most conveniently described. This adjoint coupling method allows multiple calculations using one forward and one adjoint calculation to be coupled at any desired orientation or translation.

The general coupling scheme is begun by rotating the direction cosines of the escaping particle (the U', V', W' of $\bar{\Omega}'$ at P' in Fig. 2) into the discrete ordinate coordinate system in Fig. 1 giving the U, V, W, of $\bar{\Omega}$ in the $\bar{r}, \bar{z}$ system. Since the coupling here involves forward and adjoint coordinates systems, it is the negative of the rotated adjoint direction $\bar{\Omega}'$ that must be obtained since the adjoint direction is in the opposite sense as the forward direction. Then,

$$\bar{\Omega} = -\bar{\bar{A}}\bar{\Omega}' \ , \tag{2}$$

where $\bar{\bar{A}}$ is the 3×3 rotation matrix placing the $\bar{x}'$ axis parallel to and in the same sense of the $\bar{r}$ axis, the $\bar{z}'$ axis parallel to and in the same sense of the $\bar{z}$ axis, and the $\bar{y}'$ parallel to and in the same sense of the $\bar{y}$ axis of Fig. 1.

The matrix in Eq. (2) is the inverse of the matrix required for rotating the unprimed system into the primed system, such as would be necessary if two forward calculations were being coupled. Further discussions of rotation matrix properties are given in the appendix.

Next, the position of the escaping particle x', y', z' is made relative to the coupling reference point P_c'. Then a new position vector $\bar{\rho}''$ is defined as

$$\begin{aligned} x'' &= x' - x_c' \ , \\ y'' &= y' - y_c' \ , \end{aligned} \tag{3}$$

and

$$z'' = z' - z_c' \ .$$

A final position vector $\bar{P}$ defining x, y, z in the discrete ordinates system is given by

$$\bar{\rho} = \bar{\bar{A}}\bar{\rho}'' + \bar{\rho}_c \ , \tag{4}$$

ORNL-DWG 90M-7297

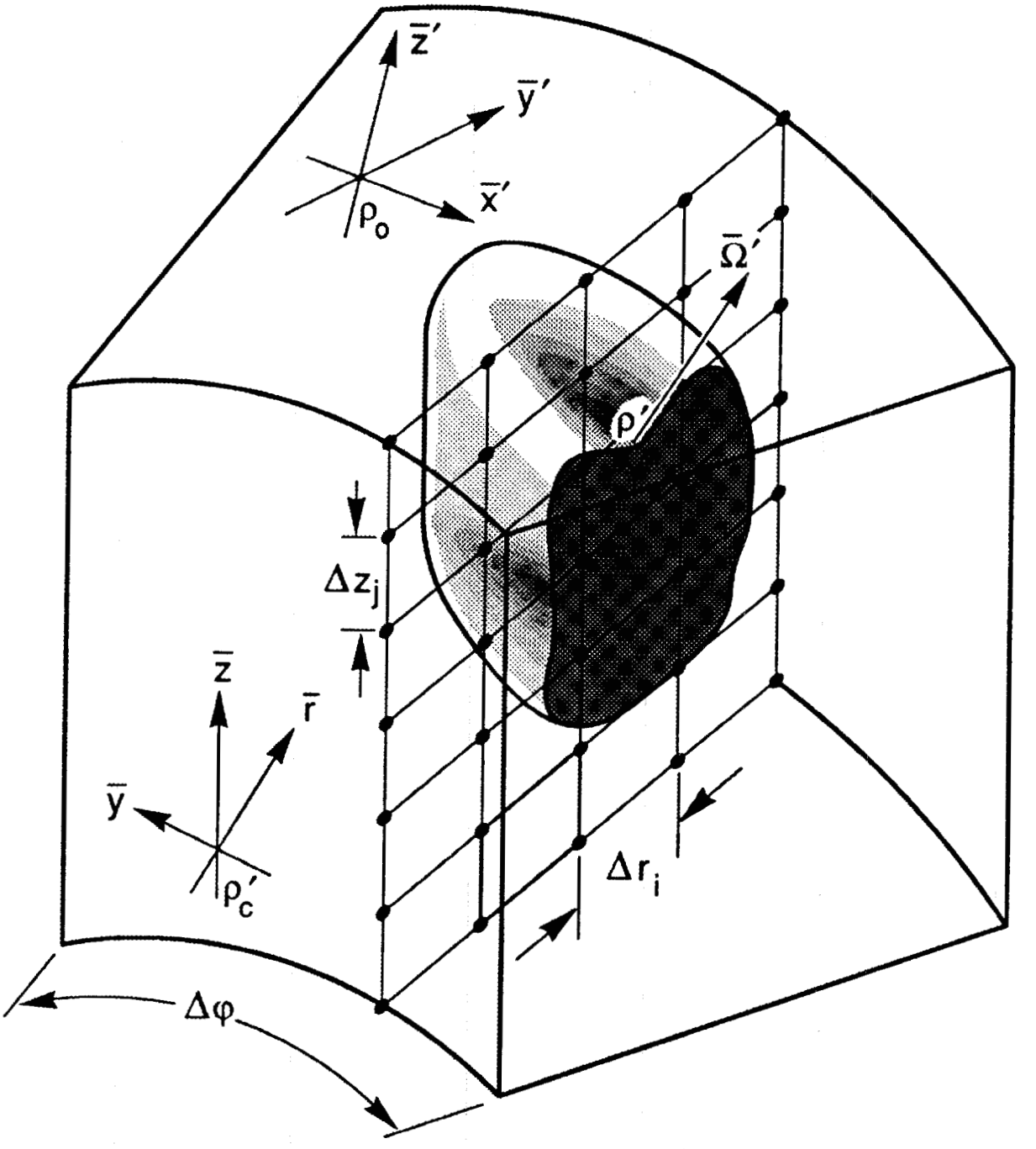

Figure 2. Monte Carlo geometry and discrete ordinates flux grid.

where x_c is the radial coordinate of the coupling point P_c on $\bar{r}, y_c = 0$, and z_c is the axial coordinate on an axis parallel to $\bar{z}$. The $\bar{\rho}$ and $\bar{\Omega}$ now represent the position on the coupling surface and the direction into the interior of the surface at that position in the discrete ordinates system. The z value from Eq. (4) determines the Δz_i from the flux grid in Fig. 2, and $r = \sqrt{x^2 + y^2}$ determines the Δr_i.

The entire coupling procedure is greatly simplified if there is no rotation of the $\bar{z}'$ axis, i.e., $\bar{z}'$ is parallel to and has the same sense of the $\bar{z}$ axis. This situation is shown in Fig. 3 where the rotated system is defined by the rotation of the positive $\bar{x}'$ axis (primed systems) counter-clockwise from the outward radial direction (unprimed systems) through the angle ϕ. From Eq. (2),

$$\begin{pmatrix} U \\ V \\ W \end{pmatrix} = -\begin{pmatrix} \cos\phi & -\sin\phi & 0 \\ \sin\phi & \cos\phi & 0 \\ 0 & 0 & 1 \end{pmatrix} \begin{pmatrix} U' \\ V' \\ W' \end{pmatrix} , \tag{5}$$

and

$$\begin{pmatrix} x \\ y \\ z \end{pmatrix} = \begin{pmatrix} \cos\phi & -\sin\phi & 0 \\ \sin\phi & \cos\phi & 0 \\ 0 & 0 & 1 \end{pmatrix} \begin{pmatrix} x' & - & x'_c \\ y' & & \\ z' & - & z'_c \end{pmatrix} + \begin{pmatrix} x_c \\ 0 \\ z_c \end{pmatrix} . \tag{6}$$

The procedure for a general rotation of the $\bar{x}', \bar{y}', \bar{z}'$ system is given in the appendix.

The Δz_i and Δr_i in Fig. 2 are determined from Eq. (6) as

$$z_j \leq z < z_{j+1} , \qquad j = 1, .., J-1 ,$$

and (7)

$$r_i \leq \sqrt{x^2 + y^2} < r_{i+1} , \qquad i = 1, ..., I-1 ,$$

where J and I are the number of axial and radial intervals necessary to completely surround the coupling surface at a specific orientation.

The x', y', z' of the escaping particle are translated to x, y, z in Eq. (6) and then related to the discrete ordinate spatial mesh from Eq. (7). However, the U, V, W from Eq. (5) must undergo an additional rotation in order to relate the U', V', W' to the discrete ordinate direction $\bar{\Omega}_{lm}$. This direction is specified by an angle α_l between $\bar{\Omega}_{lm}$ and the $+\bar{z}$ axis and an angle β_{lm} between $\bar{\Omega}_{lm}$ the outward radial direction as shown in Fig. 4. This coordinate system is superimposed onto the system in Fig. 3 at P', and the direction cosines η and μ are defined such that,

ORNL-DWG 90M-7299

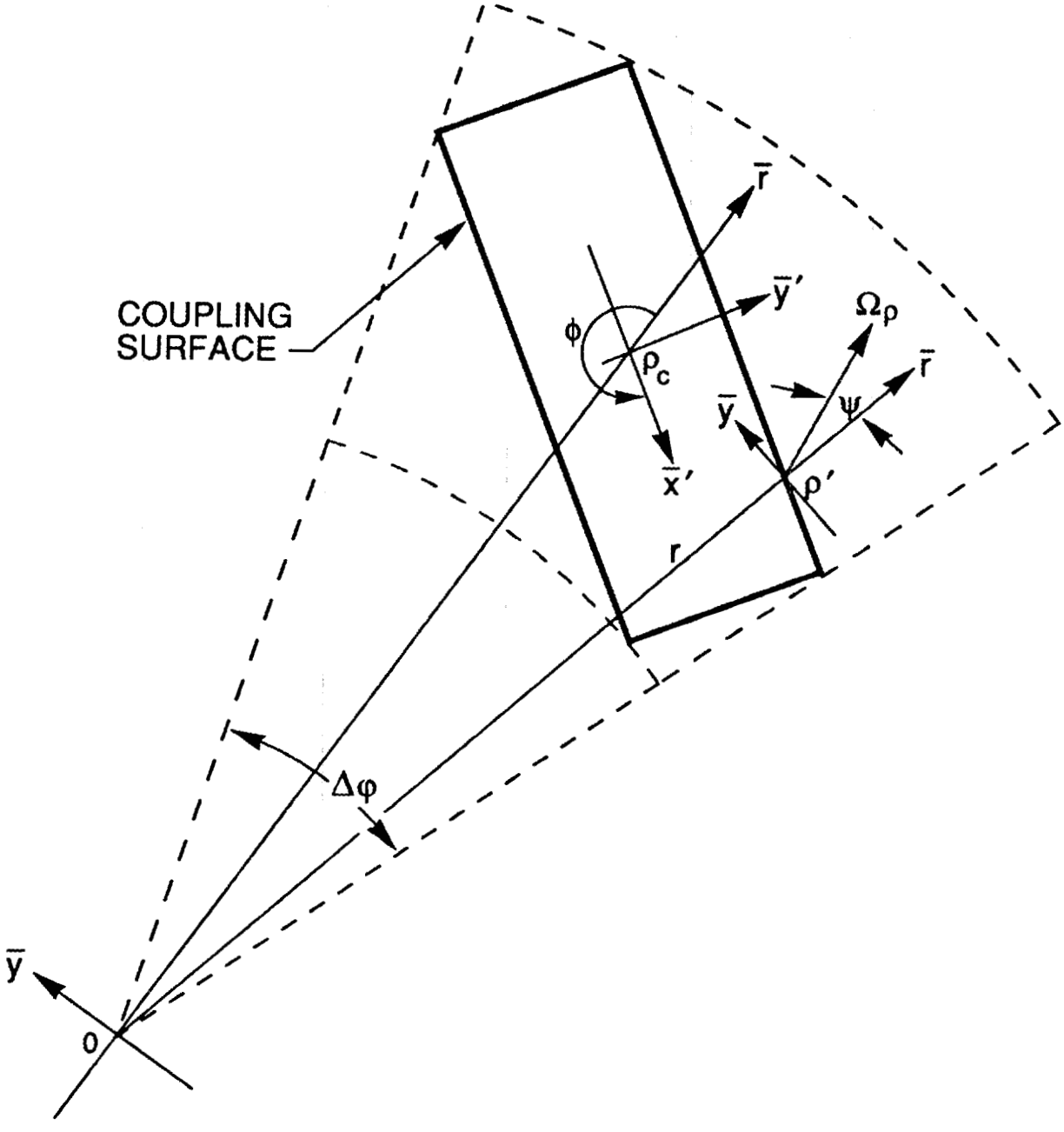

Figure 3. Horizontal projection of the coupling system geometry.

ORNL-DWG 90M-7300

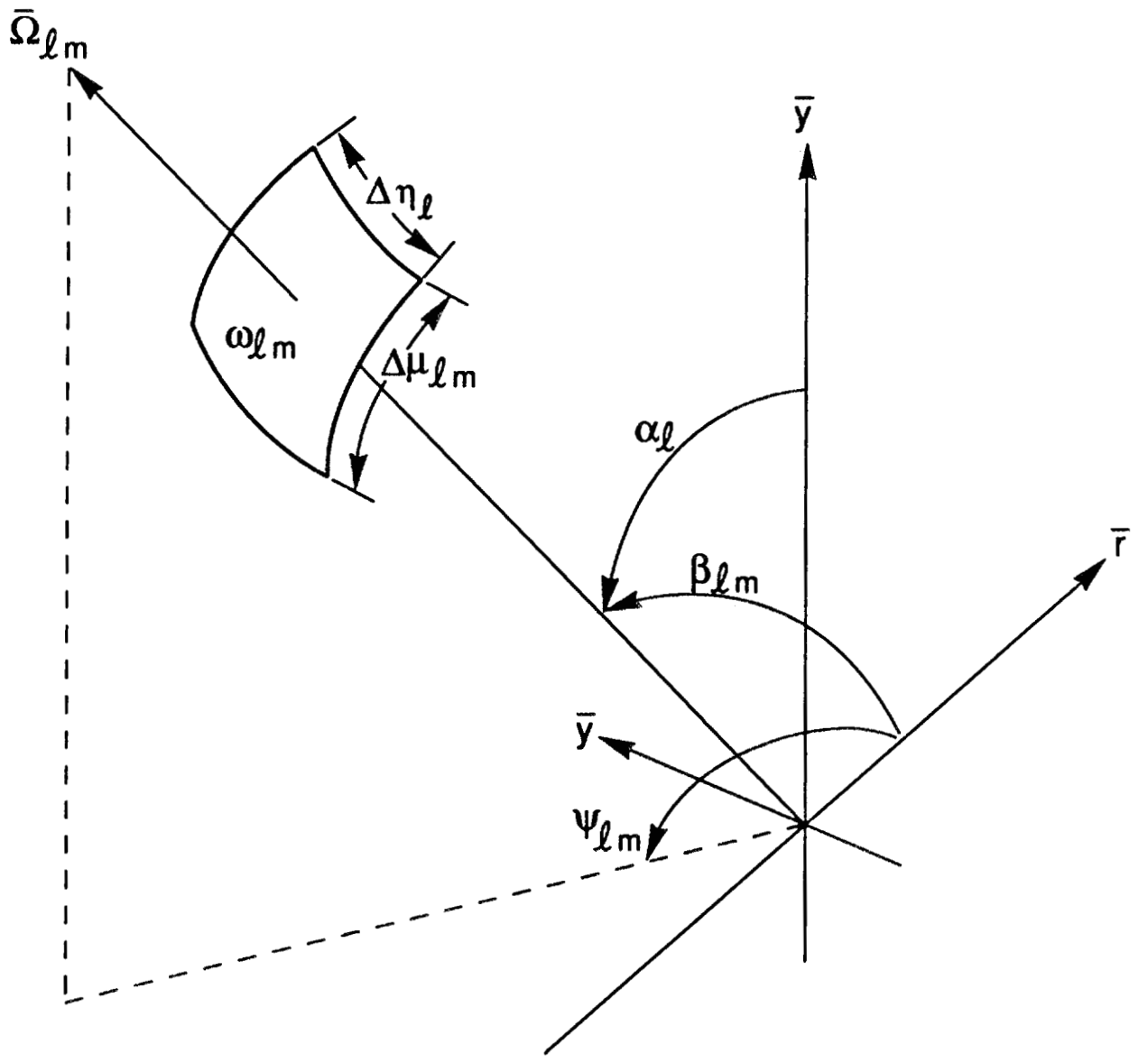

Figure 4. Discrete ordinates angular system.

$$
\begin{aligned}
\eta &= \cos\alpha_l = \bar{\Omega}\cdot\bar{z} = W \ , \\
\text{and } \mu &= \cos\beta_{lm} = \bar{\Omega}\cdot\bar{r} \\
&= U\frac{x}{\sqrt{x^2+y^2}} + V\frac{y}{\sqrt{x^2+y^2}} \ ,
\end{aligned}
\tag{8}
$$

where x and y are the coordinates in the discrete ordinates system at point P' evaluated from Eq. (6), and U, V, W are from Eq. (5). From the projection of $\bar{\Omega}$ onto the $\bar{r}, \bar{y}$ plane in Fig. 3, ψ is the angle between Ω_p and the outward radial vector. Then

$$\mu = \sqrt{1-\eta^2}\cos\psi \ ,$$

and (9)

$$\psi = \cos^{-1}\left[\frac{Ux+Vy}{\sqrt{1-W^2}\sqrt{x^2+y^2}}\right] .$$

This value of the angle ψ and the angle cosine μ are then compared to the discrete ordinates values to determine the forward flux value associated with the escaping adjoint particle. The discrete ordinate angular dependence is given in terms of discrete directions $\bar{\Omega}_{lm}$ defined by the direction cosines η_l and μ_{lm}. The direction is associated with a fractional solid angle ω_{lm} shown as an area on the unit sphere in Fig. 4. The ω_{lm} are arranged on the unit sphere with m azimuthal values given for each polar angle l. The number of azimuthal angles per polar angle increases with increasing polar angle. The limits of the solid angle fraction are used to determine within which fractional area the Monte Carlo particle escapes. The limits are determined as follows for the azimuthal angle

$$\psi_{il} = \pi\left(1-\frac{\sum_{j=1}^{i_l}\omega_{lj}}{\sum_{j=1}^{m_l}\omega_{lj}}\right) \ , \ \begin{array}{lcl} i_l & = & 1,..,.m_l \\ \psi_{l_m} & = & 0 \end{array} \ , \tag{10}$$

where m_l is the number of azimuthal values per polar value l. For the polar angle cosine,

$$\eta_l = -1+2\left(\frac{\sum_{k=1}^{l}\sum_{j=1}^{m_k}\omega_{kj}}{\sum_{k=1}^{L}\sum_{j=1}^{m_k}\omega_{kj}}\right) \begin{array}{lcl} l & = & 1,...,L \ . \\ \eta_L & = & 1 \end{array} \tag{11}$$

The polar index l is the chosen from the L polar angle cosines as

$$\eta_{l-1} < W \leq \eta_l \quad ,1 \leq l \leq L \ , \tag{12}$$

where W is from Eq. (5) and $\eta_0 = -1$. The azimuthal index i_l is chosen from the m_l azimuthal angles for the polar index l as

$$\psi_{i_l} \leq \psi < \psi_{(i-1)_l} \ , \ 1 < i_l \leq m_l \ , \tag{13}$$

where ψ is from Eq. (9) and $\psi_{0_l} = \pi$. It is the selection of the azimuthal index in Eq. (13) that represents the coupling of the three-dimensional (Monte Carlo) system to the two-dimensional (discrete ordinates) system. In the evaluation of μ in Eq. (8) the same numerical value is obtained for values of $\bar{\Omega}'$ which are mirror images across the plane of the discrete ordinate flux grid. The value of ψ from Eq. (9) is then compared with ψ_{i_l} from Eq. (10) only for azimuthal angles between 0 and π measured from the outward radial direction.

The final index necessary for the determination of the forward discrete ordinates flux in Eq. (1) is the energy group number g corresponding to the group number g' of the adjoint particle escaping the coupling surface at P'. For a group structure of N total groups, the standard forward-adjoint group inversion is

$$g = N - g' + 1 \ . \tag{14}$$

The calculation of the forward group dependent flux $\phi_{\bar{g}}$ at the detector point r_0 (the adjoint source) from which any desired response can be determined is

$$\phi_{\bar{g}} = 4\pi N \sum_{g} \int\limits_{\substack{\text{coupling}\\ \text{surface}}} \int\limits_{\bar{n}\cdot\bar{\Omega}>0} J^*_{\bar{g}g'} \phi_g(\bar{r}, \bar{\Omega}) d\bar{r} d\bar{\Omega} \ , \tag{15}$$

where $J^*_{\bar{g}g'}$ is the adjoint current (particle weight) for energy group g' at escape for a particle whose source group $\bar{g}$ was chosen uniformly from within the N groups of the group structure. If the discrete ordinates flux ϕ_g is given in terms of unit weight, as in the DOT code, rather than steradiaus, then the 4π term does not appear in Eq. (15). The MORSE code includes the N value for adjoint calculations as a standard precedure.

The discrete ordinates flux $\phi_g(\bar{r}, \bar{\Omega})$ in Eq. (15) is determined from the four fluxes at the nodes of the flux grid surrounding point P' in Fig. 2, each flux ϕ_{gij} being that for the direction $\bar{\Omega}_{lm}$ determined from the indices in Eqs. (12) and (13). Assuming linear interpolation in both radial and axial variables and using the spatial indices from Eq. (7),

$$\begin{aligned}\phi_g(\bar{r}, \bar{\Omega}) = &\left(\frac{r_i - r}{r_i - r_{i-1}}\right)\left(\frac{z_j - z}{z_j - z_{j-1}}\right)\phi_{g(i-1)(j-1)} + \left(\frac{r - r_{i-1}}{r_i - r_{i-1}}\right)\left(\frac{z_j - z}{z_j - z_{j-1}}\right)\phi_{gi(j-1)} \\ &+ \left(\frac{r_i - r}{r_i - r_{i-1}}\right)\left(\frac{z - z_{j-1}}{z_j - z_{j-1}}\right)\phi_{g(i-1)j} + \left(\frac{r - r_{i-1}}{r_i - r_{i-1}}\right)\left(\frac{z - z_{j-1}}{z_j - z_{j-1}}\right)\phi_{gij}\end{aligned} \ . \tag{16}$$

The $4\pi N$ term in Eq. (16) is from the adjoint source normalization for the point source.[4] Different normalization terms would appear for volume or surface adjoint sources. If the adjoint source group had been selected from an actual response function, then the summation of Eq. (14) over $\bar{g}$ would give this response directly. Equation (15) can be evaluated simultaneously for any orientation of the $\bar{x}', \bar{y}', \bar{z}'$ system relative to the $\bar{r}, \bar{z}$ system in Fig. 3 using the same $J^*_{\bar{g}g'}$ and the discrete ordinate flux grid.

There are other possible procedures for evaluating the discrete ordinate fluxes. A simpler angular procedure is to pick the direction $\bar{\Omega}_{lm}$ which has the largest scalar (dot) product with $\bar{\Omega}$ (i.e., pick the closest direction to $\bar{\Omega}$). However, it has been found that in certain cases this procedure can select a direction corresponding to a different solid angle than the one actually containing $\bar{\Omega}$. A more complicated angular procedure would be interpolation of ϕ_g at $\bar{\Omega}$ from the four surrounding fluxes from a directional grid similar to the spatial grid in Fig. 4 and Eq. (16). Also, it may be more appropriate to assume the discrete ordinates flux does not vary linearly with radius, but for example, linearly with volume. Then the flux terms in Eq. (16) would include a r_i^2 term and the left side would be divided by r^2 to get ϕ_g. Neither of these proposed methods has been tested in calculations.

The procedures described here for the evaluation of Eq. (16) are extensions of those found in existing, less-general coupling codes.[5–7] These procedures were developed to calculate the radiation levels in large concrete building resulting from the nuclear weapon bursts at Hiroshima and Nagasaki. Another coupling scheme has been developed in the general study of these Japanese cities which involves an additional coupling of human body radiation transport models inside domestic dwellings of such size that a general flux grid as in Fig. 2 is not needed (Reference 1, Volume 1, Chapter 9). A forward discrete ordinates-forward Monte Carlo coupling scheme has been developed where a Monte Carlo source is placed on each of the six surfaces of a cylindrical volume element as in Fig. 1 from a discrete ordinates flux grid.[8]

3. NAGASAKI BUILDING CALCULATION

The discrete ordinates calculation of the two-dimensional, air-over-ground free field flux for the two cities used in the coupling procedures is described in Chapter 3 of ref. 1, Vol. 1. Here, the source, air and ground composition, and cross-section libraries are discussed. Also given are continuous-energy Monte Carlo results of the free field calculation. The discrepancy reported between discrete ordinates and Monte Carlo results near ground zero has been confirmed in this study from standard MORSE code calculations using the same spatial zone spectral weighted cross-section set used in the DOT calculations in ref. 1. However, at the ground ranges for the coupling calculations here (500–1500 meters), the free field radiation calculated by both methods is in good agreement.

The most appropriate building for the dosimetry reassessment study is the Chinzei school in Nagasaki, which was used as a factory training facility at the time of the bombing. The building, shown in a post-blast photograph in Fig. 5, is located approximately 500 meters from ground zero, so the radiation levels were sufficiently high for the dosimetry study. Although the truss-supported roof and an upper floor auditorium partially collapsed, the lower floors remained structurally intact, and many individuals survived there, receiving various degrees of radiation-only injuries. Also, the radiation source from the Nagasaki weapon is well understood, relative to that for Hiroshima, adding to the validity of any calculated results.

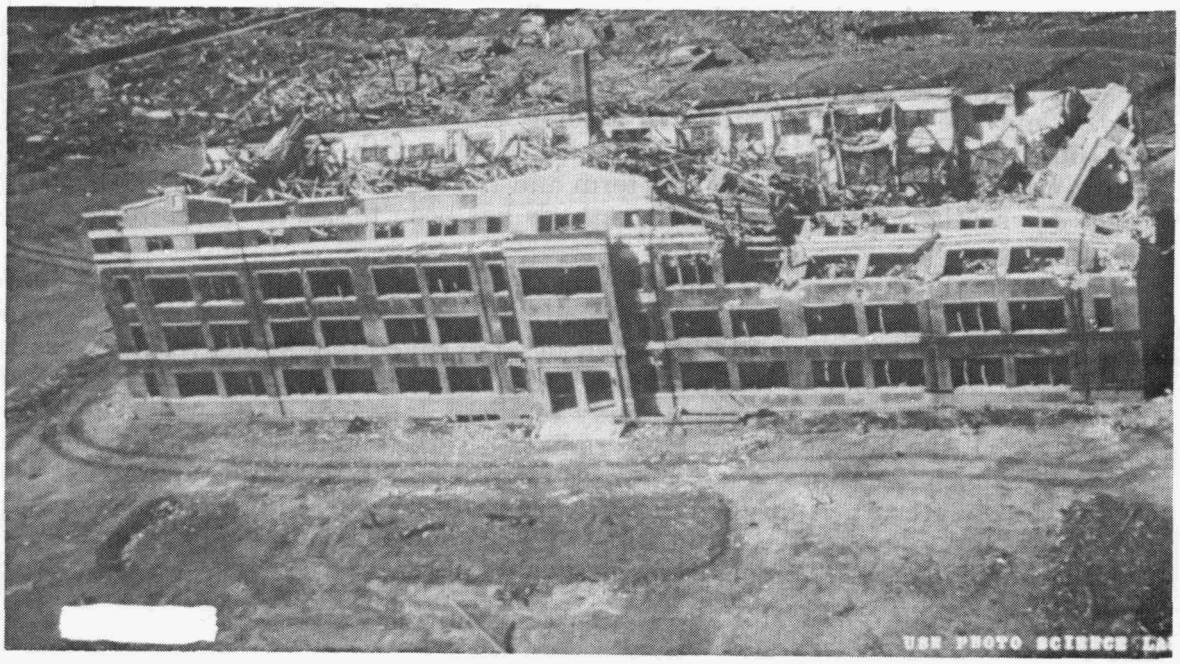

Figure 5. Reinforced concrete building in Nagasaki (Chinzei School, used as a factory machine shop).

The structure of the Chinzei school building aids in its geometric modeling. The exterior of the earthquake-resistant building has the shape of a right parallelepiped. The interior, although a maze of thick, reinforced walls, floors, columns, beams, and girders, can be modeled virtually exact with all members either parallel or perpendicular to one of the three coordinate axes.

A computer mock-up for the Monte Carlo model of the building[9,10] is shown in Fig. 6. The picture is drawn at the approximate orientation relative to the weapon burst location, 500 meters above ground zero. The vertical and horizontal lines on the exterior of the building indicate the MARS geometry array matrix[3] into which the building was modeled. The individual matrix segments were constructed

independently and placed in the array. Any identical repeating segments were modeled only once and placed in the array by appropriate translation and rotation input instructions. In this manner localized areas of the building could be modeled in greater detail to include furniture, file cabinets, bookshelves, etc., independent of the rest of the building.

ORNL-DWG 85-9780

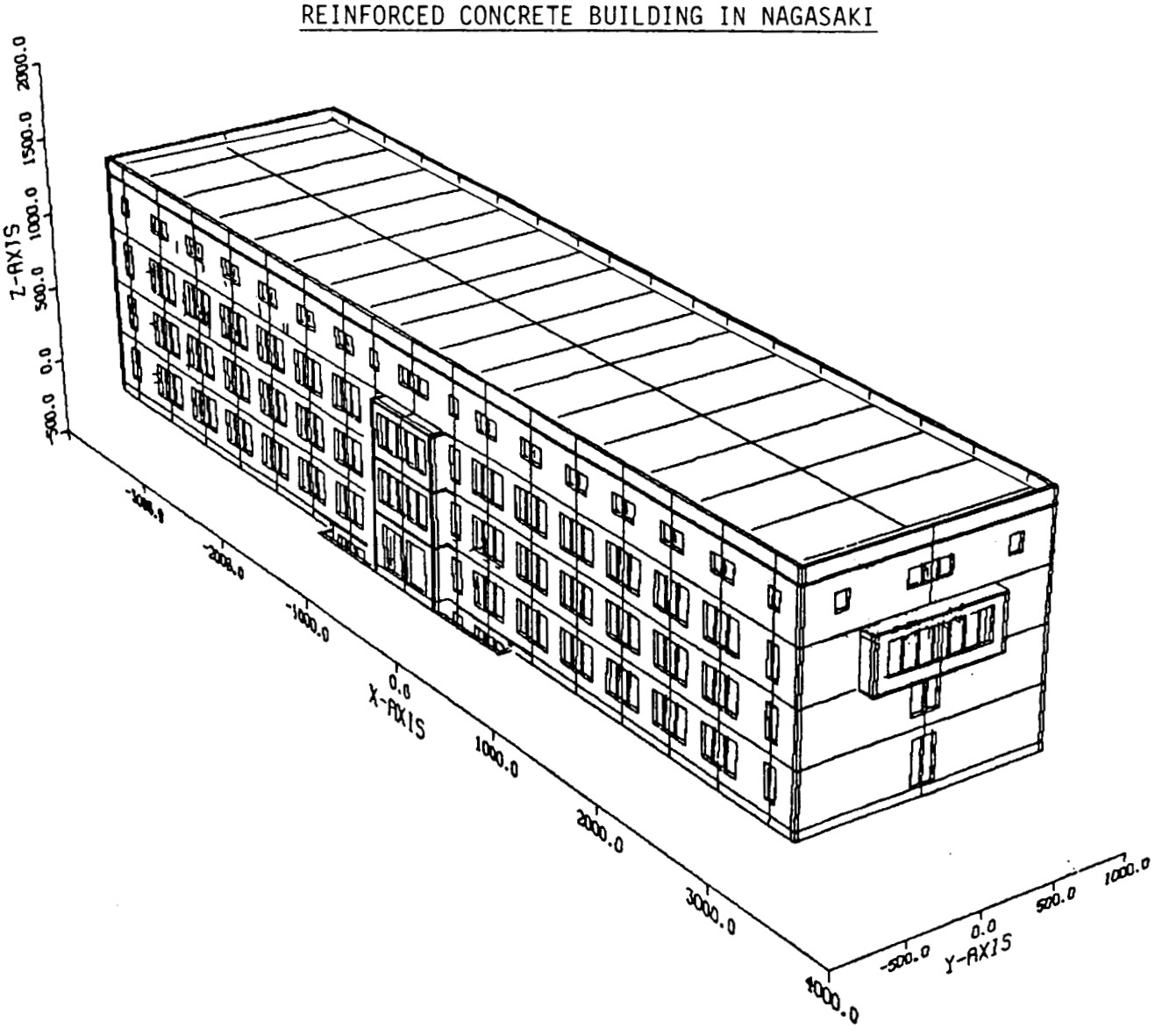

Figure 6. Computer mock-up of a reinforced concrete building in Nagasaki.

In the calculational model, adjoint particle histories are started from interior building locations and are followed until they escape across the coupling surface. The projection of this 200-m long × 140-m wide × 80-m high coupling surface surrounding the 70-m × 17-m × 14-m building is shown schematically in Fig. 5. The coupling surface was placed away from the building in an effort to ensure that the free-field, air-over-ground flux was unaffected by the presence of the building. For a high energy response wanted at a location directly exposed to the source, the exterior of the building might be used as the coupling surface; whereas, a low energy response at a location near the back side of the building would require a separation of the coupling surface from the building. The complexity of the Monte Carlo calculation here was not greatly increased by the separation of the building and coupling surface.

Depending on the starting location, various degrees of adjoint source angular biasing were used in order to direct more particles out the windows rather than through the structural material. The combined exponential transform and angular biasing schemes was used throughout the Monte Carlo calculations.[11] Special programming was also required to define spatial importance regions throughout the repeating segments of the array geometry.

The coupling procedure described in the previous section was pursued in parallel with a similar three-dimensional discrete ordinates development in the joint U.S.-Japanese government-sponsored program of dosimetric reevaluation of nuclear radiation effects. Comparisons between the Monte Carlo and three-dimensional (TORT) methods have been reported in the form of reduction factors,[12,13] i.e., the reduction in dose at a specific location in the building from the dose at the same location with no building present. These factors are given in Table 1 for a location in the center of the building 155 cm above the first floor level. In addition to the data treatment given in ref. 13 from that reported in ref. 9, an adjustment of the gamma ray factor for TORT is also in order for these comparisons. The DOT-MORSE gamma reduction factor was calculated for the weapon neutron source only, and the factor given in Table 1 is for the secondary production gamma-rays alone. However, the reported TORT results include the weapon primary gamma-ray source. Since the primary gamma-ray contribution to the total gamma ray flux at the building location in the free field data is approximately 20%, a reduction of the factor of 32 in Table 1 by an appropriate amount would bring the gamma factor comparison into the same range of agreement as for the neutron factor. However, this cannot be considered a completely linear reduction since the primary and secondary gammas contribute differently to the final result.

The Monte Carlo, two-dimensional discrete ordinates coupling method is able to produce the particle flux or dose at only one interior building location for each adjoint calculation, and while it is well suited to the exact modeling of the buildings, it could not produce the volume of results required for the dosimetry study and has remained a benchmark method. Whereas, the three-dimensional discrete ordinates method, also coupled with the same two-dimensional free-field radiation environment, produces particle flux contours throughout the interior of the coupling surface.

Table 1. Dose reduction factors for the Chinzei school building in Nagasaki for the Fat Man neutron source

	TORT	MORSE
Neutron reduction factor	13	$14 \pm 8\%$
Gamma ray reduction factor	32*	$27 \pm 12\%$

*Primary gamma ray source included. A 20% reduction gives a factor of 26.

4. HIROSHIMA NUCLIDE ACTIVATION CALCULATIONS

The transport calculation coupling scheme described in Section II has also been used for nuclide activation calculations in Hiroshima. The different amounts of activation of the same isotopes at different ground ranges have been studied in an effort to better define the Little Boy weapon output spectra and yield. In particular, the production of Co-60 from the cobalt in iron samples has been calculated and compared to measured values. The variation of these comparisons as a function of ground range is one indication of the uncertainty still existing in the understanding of the Hiroshima radiation environment.[1]

The coupling method was used to compute the Co-60 activity in an iron railing sample from the roof of the Hiroshima City Hall at 640 meters from ground zero. The City Hall is a large L-shaped building with each wing being similar to Chinzei school in Figs. 4 and 5. Only the exterior portions of the building in the vicinity of the iron railing were modeled in the Monte Carlo calculation. The activity calculated here was approximately 20% higher than that calculated using less exact models reported in Chapter 5 of ref. 1, Vol. 1 where a calculation to measurement ratio of 0.62 is reported. However, this new calculation remains substantially lower than the measured value at this location.

In a continuing effort to resolve the Hiroshima Co-60 ratio discrepancies, further use of the coupling method has recently been used to compute Co-60 activity from iron samples taken from the roof of the Chugoku Electric Company, located 700 meters from ground zero, and from the superstructure of the Yokogawa traffic bridge, located 1300 meters from ground zero.[14] Comparison of the results of these calculations with those from measurements is pending.

Another measured activity in Hiroshima was the P-32 induced in the sulfur content of utility pole porcelain insulators found throughout the city.[1] These insulators are well represented by two-dimensional geometry models, and calculations of the P-32 activity have been made by coupling the free-field fluxes to an adjoint two-dimensional discrete ordinate calculation.[15] Calculations were also performed at selected insulator sites using the Monte Carlo adjoint method in this study, reproducing virtually the same calculated activities as for the discrete ordinates coupling.

5. CODING DETAILS AND CONCLUDING REMARKS

An adjoint Monte Carlo two-dimensional forward discrete ordinates coupling method has been developed for general application. There are no restrictions as to the placement, orientation, or size of the Monte Carlo geometric model or to the use of the free field fluxes. The method has been utilized for several calculations in the on-going reassessment of nuclear weapon radiation dosimetry in Hiroshima and Nagasaki as reported in Sections III and IV.

The coupling scheme does not combine the DOT and MORSE results directly. The VISTA code[16] is used to combine the angular fluxes from DOT and any uncollided source contribution from the GRTUNCL code.[17] The output from VISTA is only for those axial and radial locations needed to enclose the MORSE geometry on the flux grid as shown in Fig. 2. The axial and radial fluxes may be retained or omitted in any combination in creating the grid.

For each Monte Carlo particle history which escapes across the coupling surface, the spatial coordinates, direction cosines, energy group at escape, and energy group at birth are written onto a MORSE history file (collision tape). The coupling code then reads the VISTA output, sets up the spatial grid shown in Fig. 2, and creates the polar and azimuthal angle limits in Eq. (10) and (11). The fluxes output from the VISTA code are read into memory only for a pre-determined number of energy groups at a time, depending on the amount of computer memory available. The particle histories on the history file in these energy groups are then coupled with the discrete ordinates fluxes via Eq. (15). Another set of VISTA energy group fluxes is then read into memory, and the history file is processed for these energy groups. This process continues until all groups have been processed.

In addition to the normal test calculations made preliminary to any final discrete ordinate or Monte Carlo calculation, the coupling methods should also be tested. This can be done by completely describing the Monte Carlo system in terms of geometry, source, etc., and then filling with air all Monte Carlo geometry inside the coupling surface that is not also in the free-field geometry. A complete coupling code calculation with this geometry should be able to reproduce, within statistical uncertainty, the free-field spatial and energy group fluxes at any location interior to the coupling surface.

A situation sometimes requiring special attention is when the uncollided portion of the angular flux is a significant fraction of the total flux at any of the space points on the discrete ordinates flux grid in Fig. 2. The discrete direction $\bar{\Omega}_{lm}$ corresponding to the direct contribution from the source may then have a flux value much larger than any of the other directions. This uncollided direction will in general be different for different grid locations. It must be assured that sufficient particles in the Monte Carlo simulation escape the coupling surface in the solid angles corresponding to these directions so that the final results are not subject to undersampling of the uncollided free-field fluxes.

A method which can sometimes alleviate any undersampling at the coupling surface is to replace, or combine, the analog escape estimate with a next-event surface crossing estimator[9] following each source and collision event in the random walk process. Although this procedure will increase the calculation time over that for the analog method, the efficiency of the calculation may be increased.

APPENDIX A

General Coordinate System Rotation

Many codes and applications of transport geometry coupling methods, such as that presented in the text, do not require a rotation of the z axis; that is, the z axes are parallel and in the same sense in both geometries. A general matrix [$\bar{\bar{A}}$ in Eq. (2) in the text] for the rotation of all axes is given in Eq. (A-1)

$$\begin{pmatrix} U \\ V \\ W \end{pmatrix} = \begin{pmatrix} \Omega_{xx} & \Omega_{yx} & \Omega_{zx} \\ \Omega_{xy} & \Omega_{yy} & \Omega_{zy} \\ \Omega_{xz} & \Omega_{yz} & \Omega_{zz} \end{pmatrix} \begin{pmatrix} U' \\ V' \\ W' \end{pmatrix} , \qquad (A-1)$$

where U', V', W are direction cosines in the rotated (primed) system and U, V, W are direction cosines in the reference (unprimed) system. Each $\Omega_{ij}(i, j = x, y, z)$ is the direction cosine of the i axis in the rotated system relative to the j axis in the reference system.

The discussions in this appendix follow that in the text for the rotation of a previously rotated coordinate system back into the reference system. The adjoint direction reversal is omitted here.

In unit vector notation, the axes directions of the rotated coordinate system relative to the reference system are

$$\begin{aligned} \bar{x}' &= \Omega_{xx}\bar{i} + \Omega_{xy}\bar{j} + \Omega_{xz}\bar{k} \\ \bar{y}' &= \Omega_{yx}\bar{i} + \Omega_{yy}\bar{j} + \Omega_{yz}\bar{k} \ . \\ \bar{z}' &= \Omega_{zx}\bar{i} + \Omega_{zy}\bar{j} + \Omega_{zz}\bar{k} \end{aligned} \qquad (A-2)$$

Since these vectors are all mutually perpendicular the following cross product relationships hold for a right-hand rule coordinate system

$$\begin{aligned} \bar{x}' &= \bar{y}' \times \bar{z}' \\ \bar{y}' &= \bar{z}' \times \bar{x}' \ . \\ \bar{z}' &= \bar{x}' \times \bar{y}' \end{aligned} \qquad (A-3)$$

Then if two of the vectors in Eq. (A-2) are known, the third is given by Eq. (A-3). The general relationship from all three cross products in Eq. (A-3) are given in the second column in Table A-I. Some other relationships are

$$\begin{aligned} \Omega_{xx}^2 + \Omega_{xy}^2 + \Omega_{xz}^2 &= 1 \\ \Omega_{yx}^2 + \Omega_{yy}^2 + \Omega_{yz}^2 &= 1 \ . \\ \Omega_{zx}^2 + \Omega_{zy}^2 + \Omega_{zz}^2 &= 1 \end{aligned} \qquad (A-4)$$

Table A-I. Rotation matrix elements for three methods of rotation

Matrix element	Direction cosines	Rotational angles	Eulerian angles
Ω_{xx}	$\Omega_{yy}\Omega_{zz}-\Omega_{yz}\Omega_{zy}$	$\cos\phi\cos\omega-\sin\phi\sin\Theta\sin\omega$	$\cos\phi\cos\psi-\sin\phi\cos\Theta\sin\psi$
Ω_{yx}	$\Omega_{zy}\Omega_{xz}-\Omega_{xy}\Omega_{zz}$	$-\sin\phi\cos\Theta$	$-\cos\phi\sin\psi-\sin\phi\cos\Theta\cos\psi$
Ω_{zx}	$\Omega_{xy}\Omega_{yz}-\Omega_{yy}\Omega_{xz}$	$\cos\phi\sin\omega+\sin\phi\sin\Theta\cos\omega$	$\sin\phi\sin\Theta$
Ω_{xy}	$\Omega_{zx}\Omega_{yz}-\Omega_{yx}\Omega_{zz}$	$\sin\phi\cos\omega+\cos\phi\sin\Theta\sin\omega$	$\sin\phi\cos\psi+\cos\phi\cos\Theta\sin\psi$
Ω_{yy}	$\Omega_{xx}\Omega_{zz}-\Omega_{xz}\Omega_{zx}$	$\cos\phi\cos\Theta$	$-\sin\phi\sin\psi+\cos\phi\cos\Theta\cos\psi$
Ω_{zy}	$\Omega_{yx}\Omega_{xz}-\Omega_{xx}\Omega_{yz}$	$\sin\phi\sin\omega-\cos\phi\sin\Theta\cos\omega$	$-\cos\phi\sin\Theta$
Ω_{xz}	$\Omega_{yx}\Omega_{zy}-\Omega_{zx}\Omega_{yy}$	$-\cos\Theta\sin\omega$	$\sin\Theta\sin\psi$
Ω_{yz}	$\Omega_{zx}\Omega_{xy}-\Omega_{xx}\Omega_{zy}$	$\sin\Theta$	$\sin\Theta\cos\psi$
Ω_{zz}	$\Omega_{xx}\Omega_{yy}-\Omega_{xy}\Omega_{yx}$	$\cos\Theta\cos\omega$	$\cos\Theta$

Thus the matrix in Eq. (A-1) may be completed when not all of the members are specified. The determinant of the rotation matrix is unity, and it is orthogonal (the inverse is equal to the transpose). The transpose of the matrix in Eq. (A-1), is given by interchanging the i and j indices on each ω_{ij} elelment. This transposed matrix would be used to define U', V', W' in terms of U, V, W.

The reference system may also be described relative to the rotated system.

$$\begin{aligned} \bar{x} &= \Omega_{xx}\bar{i} + \Omega_{yx}\bar{j} + \Omega_{zx}\bar{k} \\ \bar{y} &= \Omega_{xy}\bar{i} + \Omega_{yy}\bar{j} + \Omega_{zy}\bar{k} \ , \\ \bar{z} &= \Omega_{xz}\bar{i} + \Omega_{yz}\bar{j} + \Omega_{zz}\bar{k} \end{aligned} \qquad (A-5)$$

and

$$\begin{aligned} \Omega_{xx}^2 + \Omega_{yx}^2 + \Omega_{zx}^2 &= 1 \\ \Omega_{xy}^2 + \Omega_{yy}^2 + \Omega_{zy}^2 &= 1 \ . \\ \Omega_{xz}^2 + \Omega_{yz}^2 + \Omega_{zz}^2 &= 1 \end{aligned} \qquad (A-6)$$

The cross product relationships in Eq. (A-3) also hold for the reference axes, producing the same terms in the second column in Table A-I.

The form of the matrix implicit in Eq. (A-2) is used in the combinatorial geometry package in MORSE[3] to describe some of the body rotations, such as for the BOX body. The MCNP code[18] also uses this general matrix form for geometry rotation, and several examples are given in the MCNP manual (Chapters 3 and 4) for procedures when less than the full matrix is specified.

A rotation matrix may also be given by angular rotation of axis, rather than by cosine components, such as for the BPP (rotated BOX) body in the MARS geometry.[19] Many rotational angle schemes are possible. One method similar to the MARS rotation is three successive rotations of the reference x, y, z system to create the x', y', z' system. There is first a rotation through angle ϕ of the x-y plane by turning the $+\bar{z}$ axis counterclockwise giving $\bar{x}''', \bar{y}''', \bar{z}'''$ with $\bar{z}''' = \bar{z}$.

The matrix for this rotation is

$$\bar{\bar{B}} = \begin{pmatrix} \cos\phi & \sin\phi & 0 \\ -\sin\phi & \cos\phi & 0 \\ 0 & 0 & 1 \end{pmatrix} \ . \qquad (A-7)$$

Next, there is a rotation through angle Θ of the $y''' - z'''$ plane by turning the $+\bar{x}'''$ axis counterclockwise giving $\bar{x}'', \bar{y}'', \bar{z}''$ with $\bar{x}'' = \bar{x}'''$. The matrix for this rotation is (using the right-hand rule for all rotations)

$$\bar{\bar{C}} = \begin{pmatrix} 1 & 0 & 0 \\ 0 & \cos\Theta & \sin\Theta \\ 0 & -\sin\Theta & \cos\Theta \end{pmatrix} \ . \qquad (A-8)$$

The final rotation is through the angle ω of the $x'' - z''$ plane by turning the $+\bar{y}''$ axis counterclockwise giving $\bar{x}', \bar{y}', \bar{z}'$ with $\bar{y}' = \bar{y}''$. The applicable matrix is

$$\bar{\bar{D}} = \begin{pmatrix} \cos\omega & 0 & -\sin\omega \\ 0 & 1 & 0 \\ \sin\omega & 0 & \cos\omega \end{pmatrix} \ . \qquad (A-9)$$

The complete rotation matrix is given by

$$\overline{\overline{T}} = \overline{\overline{D}}\,\overline{\overline{C}}\,\overline{\overline{B}} \ . \qquad (A-10)$$

The matrix $\overline{\overline{T}}$ describes the rotation for rotating the x, y, z system to the x', y', z' system. However, for the application in the text, Eq. (2), and in Eq. (A-1), it is the inverse matrix $\overline{\overline{T}}^{-1}$ that is wanted to convert U', V', W' to U, V, W. Since each of $\overline{\overline{B}}$, $\overline{\overline{C}}$, and $\overline{\overline{D}}$ is orthogonal, then $\overline{\overline{T}}$ is also orthogonal and $\overline{\overline{T}}^{-1}$ is equal to the transpose of $\overline{\overline{T}}$. The elements of this transposed matrix $\overline{\overline{\tilde{T}}}$ are given in the third column of Table A-I.

Another angular rotation system that has application in many areas of mathematical physics is that of the Eulerian angles.[20] The first two rotations are the same as for the system given above. The third Eulerian rotation is through angle ψ in the $\bar{x}'' - \bar{y}''$ plane by turning the $+z''$ axis counterclockwise giving $\bar{x}', \bar{y}', \bar{z}'$ with $\bar{z}' = \bar{z}''$. The matrix is

$$\overline{\overline{E}} = \begin{pmatrix} \cos\psi & \sin\psi & 0 \\ -\sin\psi & \cos\psi & 0 \\ 0 & 0 & 1 \end{pmatrix} \ . \qquad (A-11)$$

The final Eulerian matrix for describing U', V', W as U, V, W in the x, y, z system is the inverse of $\overline{\overline{R}} = \overline{\overline{E}}\,\overline{\overline{C}}\,\overline{\overline{B}}$. The elements of $\overline{\overline{\tilde{R}}}$ are given in the fourth column of Table A-I.

These terms of the matrix in Eq. (A-1) with either of the rotational angle elements exhibit all the properties of Eq. (A-2) through (A-6) for the cosine elements. Thus there are several methods of specifying a rotation matrix and filling in any unknown elements. If enough elements are not given to amply define the matrix, the unknown elements would normally be specified in the simplest possible method; i.e., choosing unknown axes parallel or perpendicular to known axes. If the rotational angles for any system are known, the directional matrix elements may be written down directly from Table A-I. However, geometry data is usually given in different reference and rotated systems such that it is the direction cosines of the various axes that are most easily defined. Then the various angles can be obtained, if needed, from Table A-I.

REFERENCES

1. W. C. Roesch, ed., *U.S.-Japan Joint Reassessment of Atomic Bomb Radiation Dosimetry in Hiroshima and Nagasaki*, Radiation Effects Research Foundation, Hiroshima, Japan (1987).
2. W. A. Rhoades and R. L. Childs, *An Updated Version of the DOT 4 One- and Two-Dimensional Neutron/Photon Transport Code*, ORNL-5815 (1982).
3. M. B. Emmett, *MORSE-CGA, A Monte Carlo Radiation Transport Code with Array Geometry Capability*, ORNL-6174 (1985).
4. S. N. Cramer, *Applications Guide to the MORSE Monte Carlo Code*, ORNL/TM-9355 (1985).
5. M. B. Emmett, *DOMINO-II, A General Purpose Code for Coupling DOT-IV Discrete Ordinates and Monte Carlo Radiation Transport Calculations*, ORNL/TM-7771 (1981).
6. W. A. Rhoades, *et al., Development of a Code System for Determining Radiation Protection of Armored Vehicles (The VCS Code)*, ORNL-M-4664 (1974).
7. M. B. Emmett, "MASH, The Monte Carlo Adjoint Shielding Code," pp in *Advances in Nuclear Engineering Computation and Radiation Shielding*, M. L. Hall, ed., Sante Fe, New Mexico, April 9–13, 1987.
8. Y. Hayashida, *et al., J. Nucl. Sci. Tech.*, 24(2), 89 (Feb. 1987).
9. S. N. Cramer and J. S. Tang, *Variance Reduction Methods Applied to Deep-Penetration Monte Carlo Problems*, ORNL/TM-9643 (1986).
10. S. N. Cramer, J. Gonnard, and J. S. Hendricks, *Nucl. Sci. Engr.*, 92: 280–288 (1986).
11. S. N. Cramer, *Nucl. Sci. Engr.* 98: 279–298 (1988).
12. W. A. Rhoades, R. L. Childs, and D. T. Ingersoll, "New Dose Mortality Data Based on 3-D Radiation Shielding Calculations for Concrete Buildings at Nagasaki," in *Proc. 7th ICRS, 12–16 September 1988, Bournemouth, U.K.*
13. W. A. Rhoades, R. L. Childs, and D. T. Ingersoll, *Radiation Exposure Inside Reinforced Concrete Buildings at Nagasaki*, ONRL/TM-10569 (1989).
14. J. V. Pace, III and G. D. Kerr, *Calculation of the Little Boy Atomic Bomb Cobalt Activation in Iron Samples Taken at the Yokogawa Bridge and Chugoku Electric Company, Hiroshima, Japan*, ORNL report to be published.
15. J. V. Pace, III and G. D. Kerr, Session III in *Second US-Japan Workshop for Reassessment of Atomic Bomb Radiation Dosimetry in Hiroshima and Nagasaki*, the Radiation Effects Research Foundation, Hiroshima, Japan (1984).
16. W. A. Rhoades, unpublished revision of the VISA code in reference 6.
17. R. L. Childs and J. V. Pace, III, unpublished revision of RSIC code package CCC-276/DOT 3.5.
18. J. F. Briesmeister, *MCNP—A General Monte Carlo Code for Neutron and Photon Transport—Version 3A*, Los Alamos National Laboratory report LA-7396-M, Rev. 2 (1986).

19. J. T. West and M. B. Emmett, "MARS, A Multiple Array System Using Combinatorial Geometry," Vol 3, Sect. M9 of *SCALE—A Modular Code System for Performing Standardized Computer Analysis for Licensing Evaluation*, NUREG/CR-0200(ORNL/NUREG/CSD-2) (1981), Revision 2 (1984).

20. H. G. Goldstein, *Classical Mechanics*, Addison-Wesley, Reading, Mass. (1950).

INTERNAL DISTRIBUTION

1-5. EPMD Reports Office
6. B. R. Appleton
7. J. L. Bartley
8. J. A. Bucholz
9-13. S. N. Cramer
14. M. B. Emmett
15. D. T. Ingersoll
16. J. O. Johnson
17. B. L. Kirk
18. R. A. Lillie
19. F. C. Maienschein
20. J. V. Pace
21. R. W. Roussin
22-26. C. O. Slater
27. J. S. Tang
28. D. K. Trubey
29. J. E. White
30. J. J. Dorning (Consultant)
31. R. M. Haralick (Consultant)
32. J. E. Leiss (Consultant)
33. M. F. Wheeler (Consultant)
34. N. Moray (Consulant)
35-36. Laboratory Records Department
37. Laboratory Records, ORNL-RC
38. Document Reference Section
39. Central Research Library
40. ORNL Patent Section

EXTERNAL DISTRIBUTION

41. D. Auton, Defense Nuclear Agency, Office of Radiation Policy (RARP), 6801 Telegraph Road, Alexandria, VA 22310-3398.
42. J. Baublitz, Dept. of Energy, NE-20, E-435/GTN, Washington, DC 20545.
43. S. Berk, Dept. of Energy, Office of Fusion Energy, Development and Technology, ER-533, G-256/GTN, Washington, DC 20545.
44. W. Danker, Dept of Energy, DOE-RW, RE-321, 7F-031/FORS, Washington, DC 20585.
45. Charles Eisenhower, Center for Radiation Research, National Institute for Standards and Technology, Gaithersburg, MD 20899.
46. P. Hemmig, Dept. of Energy, DOE-NE, NE-462, H-410/GTN, Washington, DC 20545.
47. D. C. Kaul, Science Applications International Corporation, 10260 Campus Point Drive, San Diego, CA 92121.
48. Maj. R. A. Kehlet, Defense Nuclear Agency, 6801 Telegraph Road, Alexandria, VA 22310.
49. J. W. Sazama, Dept. of Energy, DOE-DP, DP-242.2, A-383/GTN, Washington, DC 20545.
50. Y. Song, Dept. of Energy, DOE-EH, EH-331, J-113/GTN, Washington, DC 20545.
51. G. Szeto, DOE-NE, NE-60, 2W12/NR, Washington, DC 20585.
52. J. Vogelwede, Nuclear Regulatory Commission, Information Technology Services, Washington, DC 20555.
53. E. Wahlquist, Dept. of Energy, DOE-NE, NE-52, E-428/GTN, Washington, DC 20545.
54. R. W. Young, Defense Nuclear Agency, 6801 Telegraph Road, Alexandria, VA 22310.
55. Office of Assistant Manager for Energy Research and Development, DOE-ORO, Oak Ridge, TN 37831.
56-65. Office of Scientific and Technical Information, P.O. Box 62, Oak Ridge, TN 37831.